



Structural and Transport Properties of 1T-VSe₂ Single Crystal Under High Pressures

Dongqi Song¹, Ying Zhou^{2*}, Min Zhang², Xinyi He² and Xinjian Li^{1*}

¹Key Laboratory of Material Physics, Ministry of Education, School of Physics and Microelectronics, Zhengzhou University, Zhengzhou, China, ²Institutes of Physical Science and Information Technology, Anhui University, Hefei, China

Two-dimensional transition metal dichalcogenide 1T-VSe₂ exhibits a unique three-dimensional charge density wave (CDW) order below ~110 K at ambient pressure, which shows unusual evolution under pressure. Here we report on the high-pressure structural and transport properties of 1T-VSe₂ by extending the pressure up to 57.8 GPa, through electrical transport, synchrotron X-ray diffraction (XRD) and Raman scattering measurements, which unravel two critical pressure points. The CDW transition is found to be enhanced under compression at a rate of 16.5 K/GPa up to the first critical pressure $P_{C1} \sim 12$ GPa, at which a structural phase transition from hexagonal $P-3m1$ to monoclinic $C2/m$ phase takes place. The second critical pressure $P_{C2} \sim 33$ GPa corresponds to another structural transition from monoclinic $C2/m$ to $P2_1/m$ phase. These findings extend the phase diagram of pressurized 1T-VSe₂ and may help to understand pressure tuning of structures in transition metal dichalcogenides.

Keywords: high pressure, transition metal chalcogenides, structural phase transition, charge density wave, electrical transport

INTRODUCTION

Two-dimensional transition metal dichalcogenides (TMDs) exhibit rich physical properties, which have been a hot research field in condensed matter physics for both fundamental interests and potential applications in electronics and optoelectronics (Sipos et al., 2008; Choi et al., 2013; Nayak et al., 2014; Novoselov et al., 2016). Among them, 1T-VSe₂ has attracted extensive interests due to its unique three-dimensional (3D) charge density wave (CDW) order (Tsutsumi, 1982; Terashima et al., 2003; Strocov et al., 2012; Jolie et al., 2019), intrinsic photocatalytic (He et al., 2017) and photoluminescence properties (Ghobadi et al., 2018). Bulk 1T-VSe₂ has a hexagonal layered structure, namely 1T ($P-3m1$) phase. The adjacent Se-V-Se sandwiches are held together by van der Waals interactions, and each V atom is surrounded by the nearest six Se atoms, constituting VSe₆ octahedron **Figure 1A** (van Bruggen and Haas, 1976). It exhibits an incommensurate CDW with $4a \times 4a \times 3.18c$ periodic lattice distortion upon cooling to around 110 K, followed by a second transition to a commensurate CDW state at ~80 K (Thompson and Silbernagel, 1979; Tsutsumi, 1982; Eaglesham et al., 1986; Terashima et al., 2003; Pandey and Soni, 2020). The mechanism of the 3D CDW was initially explained by Fermi-surface nesting resulting from the warped 3D electron pocket centered around the M point at the edge of the Brillouin zone (Terashima et al., 2003; Sato et al., 2004; Strocov et al., 2012). Recently, electron-phonon coupling was also found to contribute to the formation of the CDW (Pandey and Soni, 2020; Si et al., 2020). Previous studies showed that the valence band structure of 1T-VSe₂ can be transformed into two-dimensional (2D) character by alkali metal intercalation, which was attributed to charge transfer and decoupling of the layers induced by

OPEN ACCESS

Edited by:

Mingliang Tian,
Hefei Institutes of Physical Science
(CAS), China

Reviewed by:

Liling Sun,
Institute of Physics (CAS), China
Jie Ma,
Shanghai Jiao Tong University, China

*Correspondence:

Ying Zhou
yzhou@ahu.edu.cn
Xinjian Li
lixj@zzu.edu.cn

Specialty section:

This article was submitted to
Quantum Materials,
a section of the journal
Frontiers in Materials

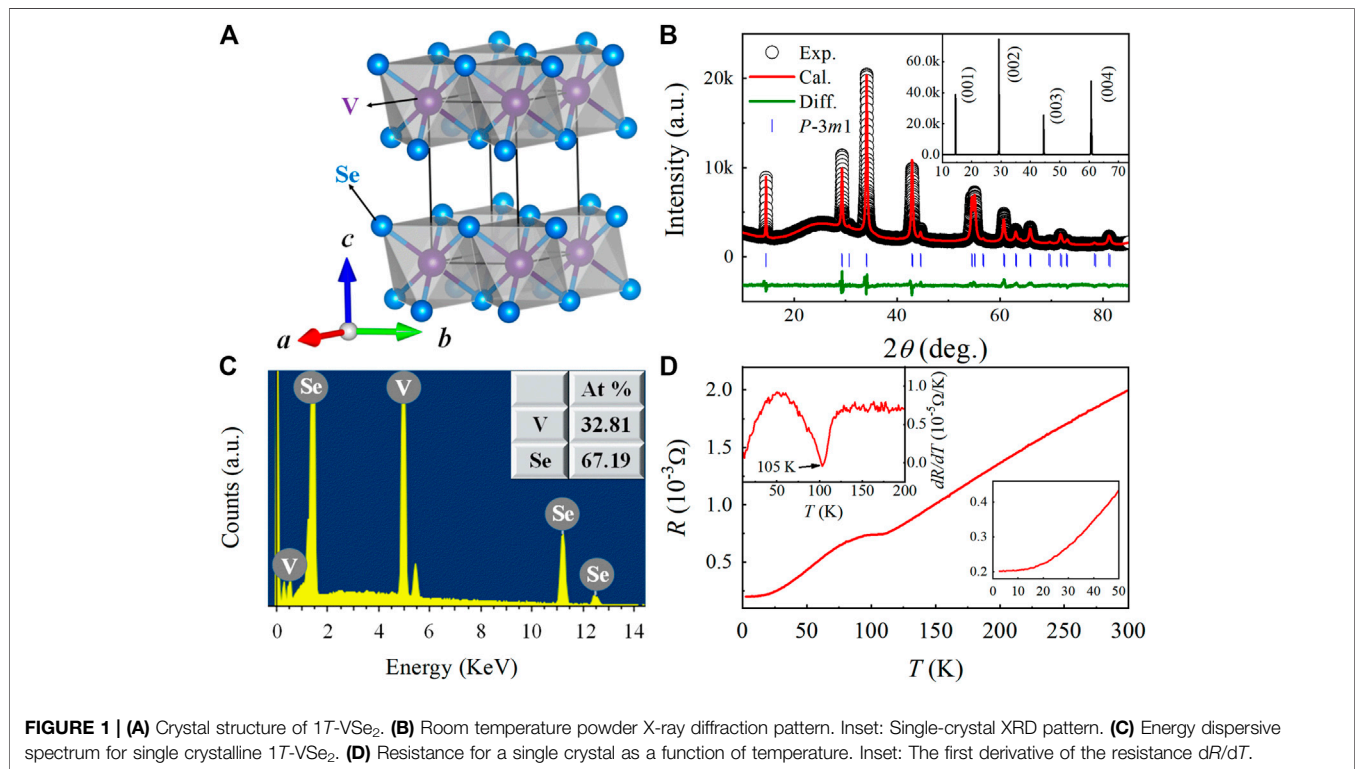
Received: 17 May 2021

Accepted: 08 June 2021

Published: 30 June 2021

Citation:

Song D, Zhou Y, Zhang M, He X and
Li X (2021) Structural and Transport
Properties of 1T-VSe₂ Single Crystal
Under High Pressures.
Front. Mater. 8:710849.
doi: 10.3389/fmats.2021.710849



the intercalated alkali ions (Starnberg et al., 1993; Brauer et al., 1998). In addition, the CDW ordering temperature can also be tuned effectively by the reduction of sample thickness owing to reduced interlayer coupling and enhanced quantum confinement (Yang et al., 2014; Pásztor et al., 2017). At the monolayer limit, many interesting phenomena have been reported, such as ferromagnetism (Ma et al., 2012; Bonilla et al., 2018), distinct CDW order (Zhang et al., 2017; Feng et al., 2018; Duvjir et al., 2018) as well as Mott/Peierls insulating state (Duvjir et al., 2018; Umemoto et al., 2018), depending on preparation conditions.

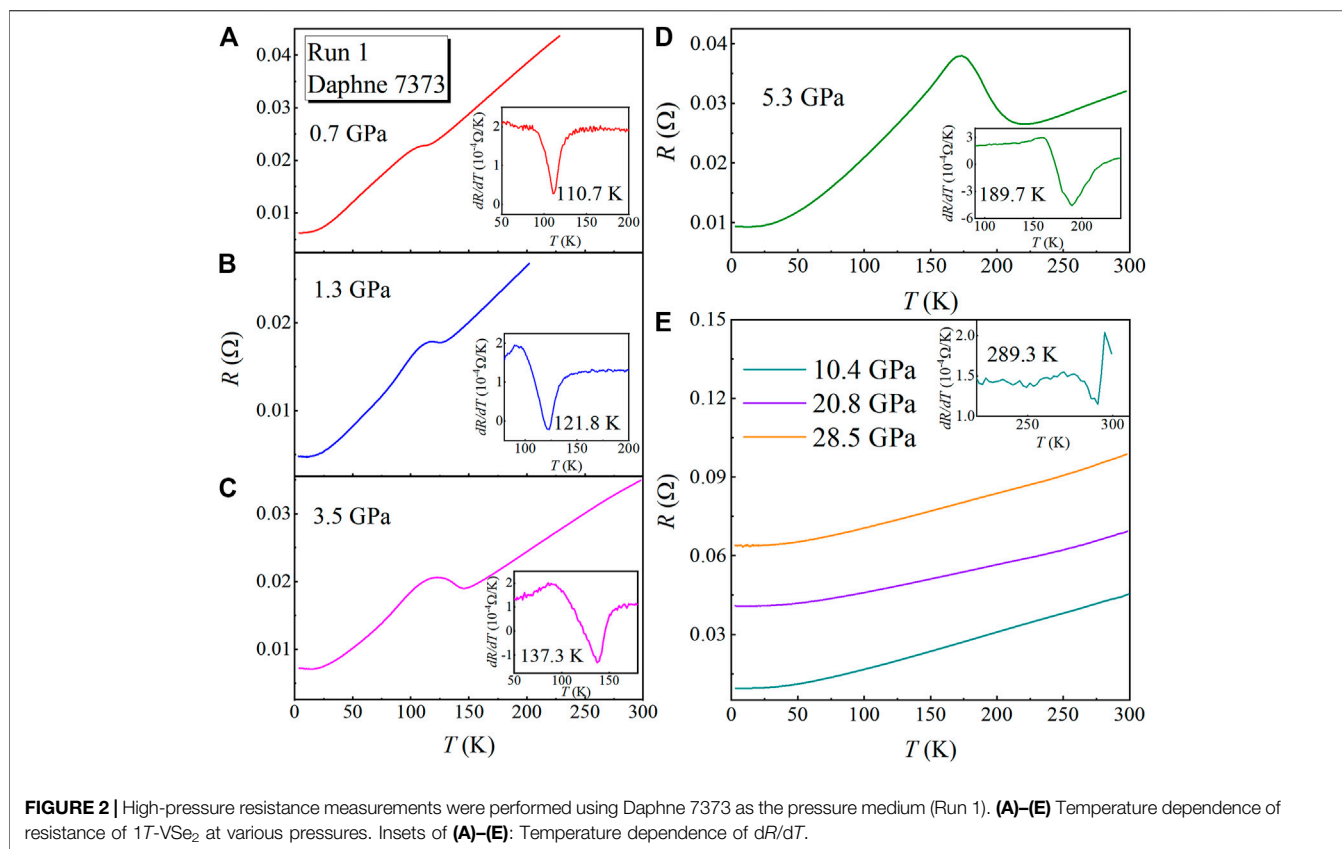
Pressure has been considered as a clean and effective method to tune lattice degrees of freedom, and thereby the physical properties of materials (Mao et al., 2018). In 1T-VSe₂, a pressure-induced structural phase transition from 1T phase to monoclinic C2/m phase with a novel superstructure around 15 GPa were reported *via* theoretical calculations, Raman spectroscopy and synchrotron X-ray diffraction (XRD) (Sereika et al., 2020; Feng et al., 2020). As for the transport properties of 1T-VSe₂ under pressure, controversial results have been reported. Specifically, Sahoo *et al.* reported that the CDW transition temperature (T_{CDW}) first increases marginally up to 5 GPa and then increases rapidly, and accompanying by non-hydrostatic pressure-induced suppression of CDW, superconductivity emerges at ~ 15 GPa (Sahoo et al., 2020). However, soon after, Feng *et al.* found that the CDW transition temperature was enhanced linearly by increasing pressure, reaching 358 K at 14.6 GPa and no superconducting transition is observed under quasi-hydrostatic pressure up to

29.6 GPa (Feng et al., 2020). Obviously, the detailed properties of 1T-VSe₂ under pressure remain far from being well explored. In addition, in these reports, the pressures applied in the XRD, Raman, and resistance measurements are below 30–35 GPa (Friend et al., 1978; Sereika et al., 2020; Feng et al., 2020; Sahoo et al., 2020). For pressures above 35 GPa, the evolution of structural and transport properties are still unclear.

In this paper, we synthesize high-quality 1T-VSe₂ single crystals and investigate the evolution of structural and transport properties under pressure up to 57.8 GPa. Resistance measurements show that the T_{CDW} shifts gradually to higher temperature with increasing pressure up to $P_{\text{C1}} \sim 12$ GPa, at which the hexagonal P-3m1 structure undergoes a transition to monoclinic C2/m phase. And no sign of superconductivity is observed in the pressurized 1T-VSe₂ up to 42 GPa. Moreover, our synchrotron XRD and Raman experiments reveal a second structural transition from the monoclinic C2/m to P2₁/m phase with further increasing pressure to the second critical pressure $P_{\text{C2}} \sim 33$ GPa.

MATERIALS AND METHODS

Single crystals of 1T-VSe₂ were synthesized by chemical vapor transport method using selenium (about 2 mg/cm³) as transport agent (van Bruggen and Haas, 1976). The mixture of Vanadium (3N) and Selenium (5N) powders was sealed in an evacuated quartz tube. Then the quartz tube was heated for 1 week in a two-



zone furnace with a temperature field of $\Delta T = (850\text{--}780)^\circ\text{C}$. The structure of the single-crystalline samples was analyzed by XRD experiments with Cu-K α radiation ($\lambda = 1.5418 \text{ \AA}$). The atomic ratio was characterized by the energy dispersive X-ray spectrometry. The temperature-dependent resistance was measured using a standard four-point-probe method.

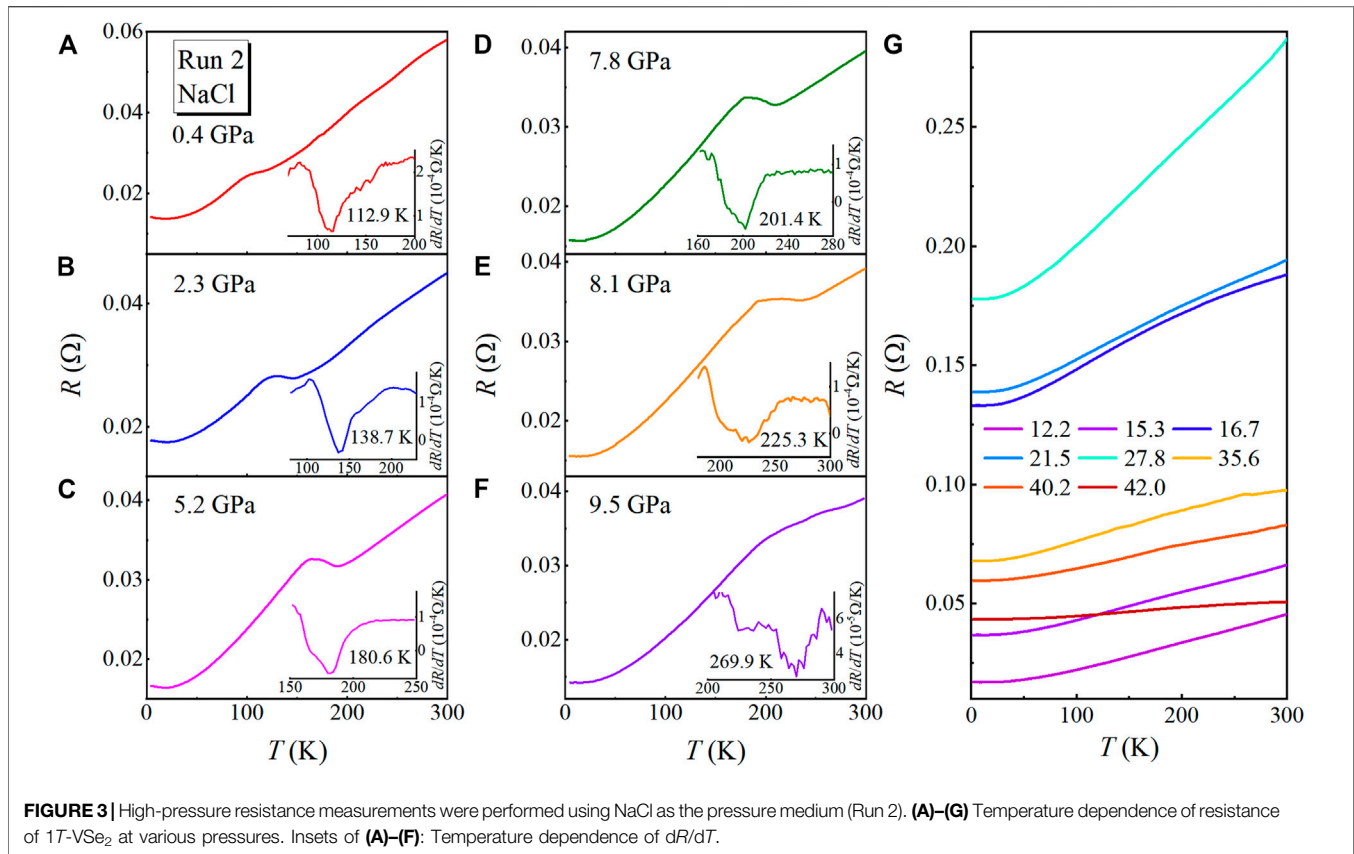
High-pressure resistance measurements were performed in a nonmagnetic Be-Cu diamond anvil cell (Zhou et al., 2019). Diamond anvils of 300 μm culets and a T301 stainless-steel gasket covered with a mixture of epoxy and fine cubic boron nitride (c-BN) powder were used. A hole with diameter of 150 μm was drilled at the center of the c-BN-covered pit, and then filled with pressure-transmitting medium. Daphne 7373 and NaCl were used as pressure-transmitting medium in Run 1 and Run 2, respectively. A rectangular single-crystal sample was loaded into the hole, together with some ruby powder as the pressure marker. Pt foils with a thickness of 7.5 μm were used as the electrode leads. The cell was then put into an in-house multifunctional physical properties measurement system. The resistance R was collected using the standard four-probe method *via* sweeping temperature.

Synchrotron XRD and Raman scattering measurements under pressure were performed in a Mao-Bell cell at room temperature. Daphne 7373 was used as pressure-transmitting medium for both experiments. The XRD was performed on powder crushed from single crystals at the beamline BL15U1 of the Shanghai

Synchrotron Radiation Facility (SSRF). The wavelength of the focused monochromatic X-ray beam is 0.6199 \AA . The DIOPTAS program (Clemens and Vitali, 2015) was used for image integrations. The XRD patterns were fitted by using the RIETICA program (Hunter, 1998) with the Le Bail method. Raman spectra were measured with a freshly cleaved 1T-VSe₂ single crystal using the 532-nm solid-state laser. The pressure was calibrated by using the ruby fluorescence shift at room temperature for all of the high-pressure experiments above (Mao et al., 1986).

RESULTS AND DISCUSSION

Figure 1B displays the XRD pattern for powdered 1T-VSe₂ single crystals. All peaks can be well indexed by the $P\text{-}3m1$ space group, and the fitting yields the cell parameters $a = b = 3.36 \text{ \AA}$, $c = 6.09 \text{ \AA}$, and $V = 59.54 \text{ \AA}^3$, in excellent accordance with the previous reports (van Bruggen and Haas, 1976; Pandey and Soni, 2020). A typical single-crystal diffraction pattern for 1T-VSe₂ is shown in the inset of **Figure 1B**. Only (00 l) reflections are observed, indicating a c -axis orientation of the cleavage plane. The energy-dispersive X-ray spectrum gives the ratio of V: Se as 1: 2.05 (**Figure 1C**). The in-plane resistance R as a function of temperature at ambient pressure is given in **Figure 1D**. The R - T curve shows an overall metallic behavior but with a clear hump



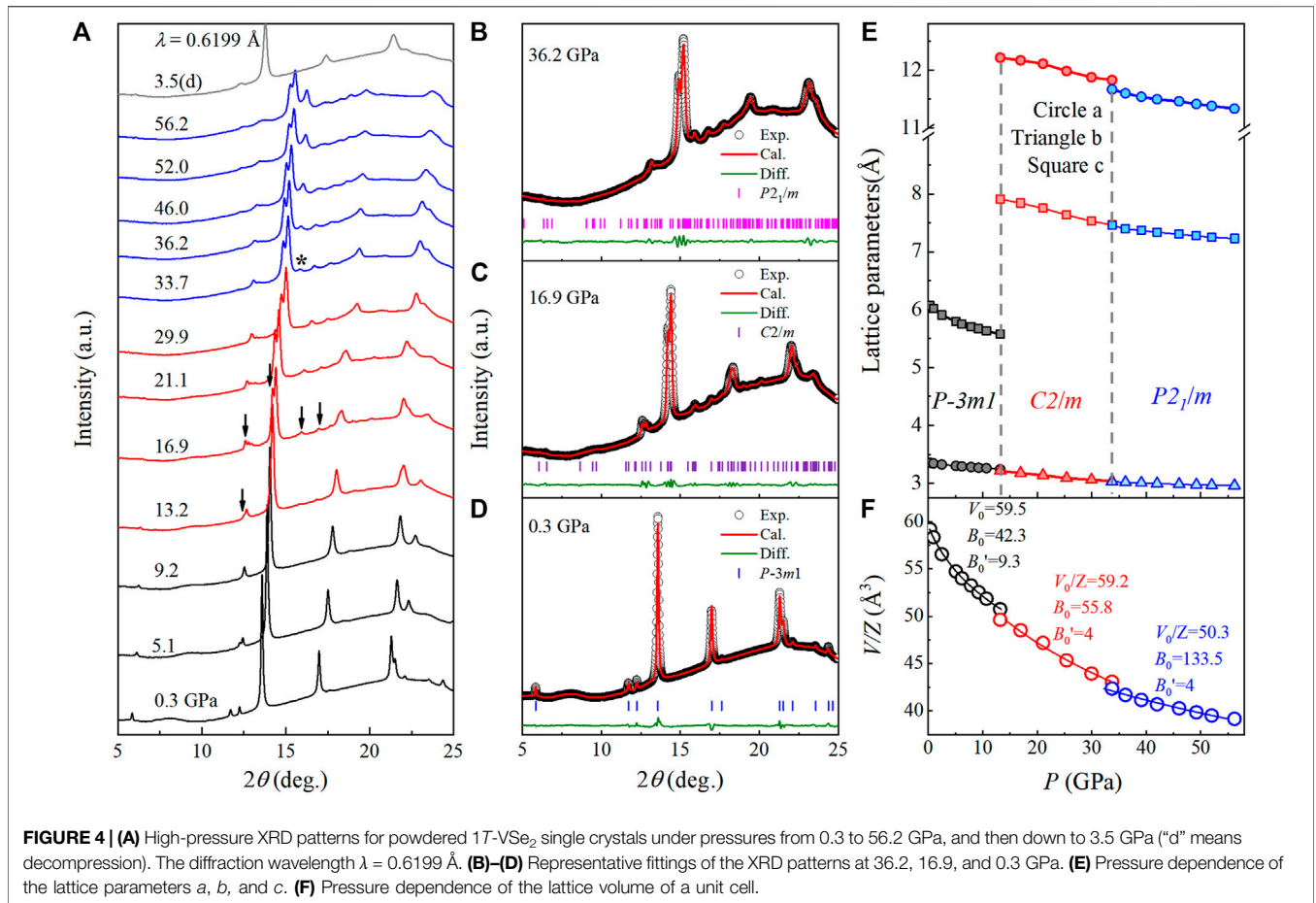
feature at around 105 K related to the CDW transition, in agreement with the previous studies (van Bruggen and Haas, 1976; Pandey and Soni, 2020). The CDW transition temperature T_{CDW} is defined as the temperature at which the dR/dT is minimum (inset of **Figure 1D**). The characterizations above indicate high quality of our samples.

To check on the pressure evolution of CDW and pressure-induced superconductivity in 1T-VSe₂, we have performed resistance measurements under pressures using different pressure-transmitting mediums. In Run 1 (**Figure 2**), we used Daphne 7373 as the pressure medium with pressures up to 28.5 GPa. As one can see in **Figure 2A**, at $p = 0.7$ GPa, a resistance hump relating to the CDW transition is observed at around 110.7 K, which is higher than that at ambient pressure (**Figure 1D**). With further increasing pressure, the temperature of the resistance hump rises rapidly and reaches a maximum of 289.3 K at $p = 10.4$ GPa. This suggests an enhancement of the CDW under pressure, in agreement with the previous reports (Friend et al., 1978; Feng et al., 2020; Sahoo et al., 2020). For pressures higher than 10.4 GPa (**Figure 2E**), the resistance hump is indiscernible, namely, no sign of CDW is observed in the temperature range of 2–300 K, and the $R(T)$ curve is monotonically shifted upwards.

For comparison, we further carried out $R(T)$ measurements using solid pressure medium (NaCl) up to 42.0 GPa in Run 2 (**Figure 3**), which is referred as non-hydrostatic pressure similar

to that in Ref. (Sahoo et al., 2020). With increasing pressure from 0.4 to 10.9 GPa, the resistance hump moves toward higher temperatures, in conformity with that of Run 1, confirming that compression can increase T_{CDW} in 1T-VSe₂. The evident enhancement of T_{CDW} could be related to the pressure-enhanced CDW gap and improvement of out-of-plane Fermi surface nesting due to increase of the dimensionality (Feng et al., 2020). Nevertheless, either quasi-hydrostatic or non-hydrostatic compression, no sign of superconductivity is observed from 2 to 300 K measured up to 42.0 GPa in our measurements.

Next, pressure evolution of crystal structure of 1T-VSe₂ was studied by synchrotron XRD measurements on powdered samples. Typical XRD patterns are shown in **Figure 4A** and three representative fittings for pressures $p = 0.3$, 16.9, and 36.2 GPa are presented in **Figures 4B–D**. Starting at 0.3 GPa, the XRD pattern can be well indexed by hexagonal crystal structure with space group $P-3m1$ (No. 164) (**Figure 4D**), which is the same as that of 1T-VSe₂ at ambient pressure. Upon compression, all peaks shift to higher angles due to shrinkage of the lattice. At $P_{C1} \sim 13.2$ GPa, some new diffraction peaks begin to occur at the 2θ angles of 12.6, 14.2, 15.9, and 17.0°, as denoted by arrows in **Figure 4A**, which indicates a structural transition. Phase II (red) can be fitted with the monoclinic $C2/m$ structure (No. 12) as shown in **Figure 4C**, which is in accord with the results of Refs. (Feng



et al., 2020; Sahoo et al., 2020). The $C2/m$ structure can be considered as a distorted 1T phase, which involves the formation of trimers associated with tiny displacement of V atoms, leading to the formation of a novel $3 \times 1 \times 1$ superstructure (Sereika et al., 2020; Feng et al., 2020). Moreover, when the pressure is increased to $P_{C2} \sim 33.7$ GPa, an additional peak appears at 15.8° (see the star in **Figure 4A**); and its intensity increases with pressure increasing, which indicates occurrence of another structural transition. It is well-known that depending on the various stacking sequences of the two-dimension layers and the coordination of transition metal atoms, two-dimensional transition metal dichalcogenides MX_2 can crystallize into different types, such as 1T ($P-3m1$), 1T' ($C2/m$ and $P2_1/m$), 2H ($P63/mmc$), 3R ($R3m$), Td ($Pmn2$) etc (Sofer et al., 2017). Excluding the ambient pressure $P-3m1$ and the first high-pressure $C2/m$ phases, there are four remaining possible structures. We tried fitting our high-pressure XRD data by these candidate structures and found that the high-pressure XRD patterns above ~ 33.7 GPa can be well fitted by the $P2_1/m$ space group (**Figure 4B**), suggesting that the newly emergent phase III (blue) is a monoclinic structure with space group $P2_1/m$ (No. 11), similar with that in pressurized TaTe₂ (Guo et al., 2017). When the pressure is released to 3.5 GPa (denoted by d, top

of **Figure 4A**), the XRD pattern evolves back to the starting structure of 1T-VSe₂, implying that these two structural transitions are reversible.

The extracted lattice parameters as a function of pressure are summarized in **Figure 4E**. The lattice parameters for $P-3m1$, $C2/m$, and $P2_1/m$ phases decrease gradually upon compression. The pressure dependence of unit cell volume V/Z is plotted in **Figure 4F**. The isothermal equations of state (EoS) were fitted by the third-order Birch-Murnaghan formula (Birch, 1947), as indicated by the solid lines. Our fitting yields the zero-pressure volume $V_0 = 59.5 \text{ \AA}^3$, bulk modulus $B_0 = 42.3$ GPa, and first-order derivative of the bulk modulus $B'_0 = 9.3$ for $P-3m1$ phase. With B'_0 fixed as 4, the calculated parameters are $V_0 = 59.2 \text{ \AA}^3$, $B_0 = 55.8$ GPa for $C2/m$ phase; and $V_0 = 50.3 \text{ \AA}^3$, $B_0 = 133.5$ GPa for $P2_1/m$ phase.

It is known that the properties of the CDW transition are closely related to the dimensionality of the material. In **Supplementary Figure S1**, we plotted the pressure-dependent T_{CDW} and the axial ratio c/a . It is obvious to see a direct correlation between the increase of T_{CDW} and decrease of c/a ratio. And the axial ratio c/a of 1T-VSe₂ decreases with pressure, that is, the dimensionality of the system increases (Feng et al., 2020). These results suggest that the enhancement of CDW is related to the inherent dimensionality of 1T-VSe₂.

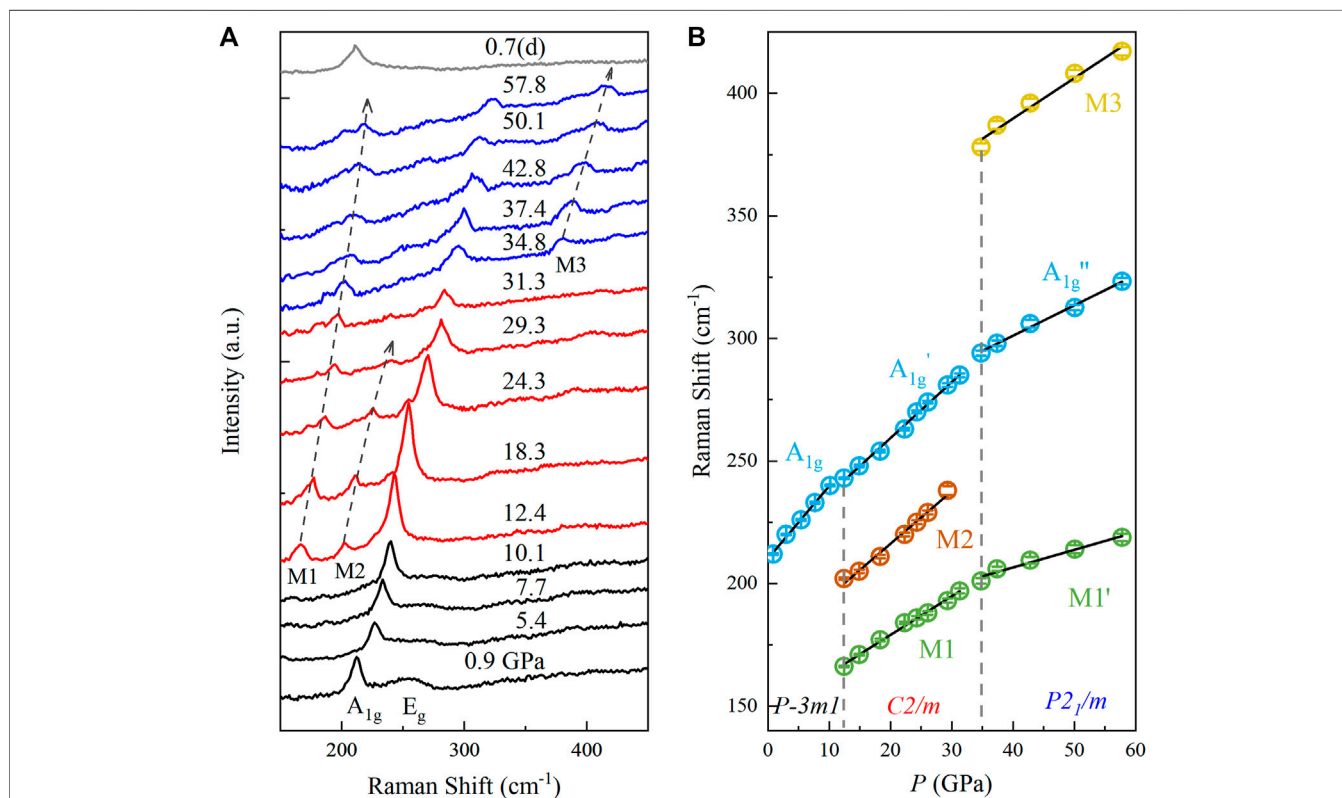


FIGURE 5 | (A) Room-temperature Raman spectra of 1T-VSe₂ single crystal under selected pressures. The Raman spectrum under decompression is labeled by “d”. The dashed lines are guides for the eye. **(B)** Pressure dependence of Raman frequencies of 1T-VSe₂. Solid lines are linear fits to data.

TABLE 1 | Pressure coefficient ($d\omega/dP$) and mode Grüneisen parameter (γ_i) for different Raman modes.

Space group	Symmetry	ω_0 (cm ⁻¹)	$d\omega/dP$ (cm ⁻¹ . GPa ⁻¹)	γ_i
<i>P-3m1</i>	A_{1g}	210.2	2.97	0.60
<i>C2/m</i>	M1	147.5	1.58	0.60
	M2	173.4	2.14	0.69
<i>P2₁/m</i>	A_{1g}'	213.6	2.28	0.60
	M1'	177.8	0.72	0.54
	A_{1g}''	251.6	1.24	0.66
	M3	323.6	1.65	0.68

Raman spectroscopy is also an effective and powerful tool in detecting structural transition. Bulk 1T-VSe₂ single-crystal displays a sharp A_{1g} mode ~ 206 cm⁻¹ along with two additional modes associated with $E_g \sim 257$ cm⁻¹ symmetry and two-phonon (2_{ph}) ~ 332 cm⁻¹ interactions at room temperature and ambient pressure (Pandey and Soni, 2020). **Figure 5A** shows the room-temperature Raman spectra of 1T-VSe₂ single crystal at selected pressures. At a pressure of 0.9 GPa, the A_{1g} and E_g modes are detected at ~ 212 cm⁻¹ and 255 cm⁻¹, respectively, in agreement with previous report (Pandey and Soni, 2020). Since the E_g mode cannot be identified accurately at the higher pressure, we only trace A_{1g} in this paper. With increasing pressure, the A_{1g} mode moves toward higher frequencies monotonically. At $P_{C1} \sim 12.4$ GPa, along with the

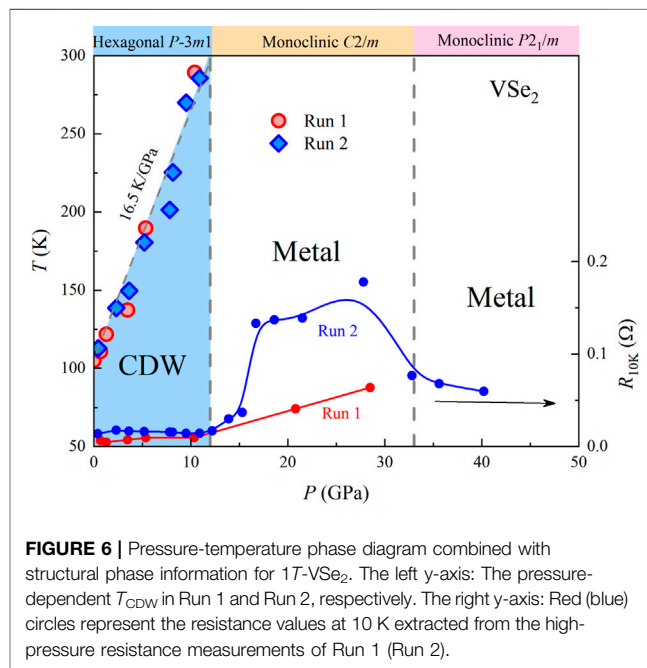


FIGURE 6 | Pressure-temperature phase diagram combined with structural phase information for 1T-VSe₂. The left y-axis: The pressure-dependent T_{CDW} in Run 1 and Run 2, respectively. The right y-axis: Red (blue) circles represent the resistance values at 10 K extracted from the high-pressure resistance measurements of Run 1 (Run 2).

structural transition to monoclinic *C2/m* structure, two new peaks are detected at 166, 202 cm⁻¹ (labeled as M1 and M2, respectively), which is consistent with the previous study (Feng

et al., 2020). Considering the continuous evolution of the A_{1g} mode and the structural phase transition, we labeled the A_{1g} mode in the range of 12.4–31.3 GPa as A_{1g}' mode. With increasing pressure up to 31.3 GPa, all A_{1g}', M1, and M2 peaks shift toward high frequency. Upon further compression above P_{C2} ~ 33 GPa, the M2 mode disappears and another peak at 378 cm⁻¹ emerges, which can be attributed to the structural transition from C2/m to P2₁/m detected in the XRD measurements. Similarly, we labeled the M1 and A_{1g}' modes above 31.3 GPa as the M1' and A_{1g}'' modes, respectively. The remaining one is labeled as M3. The Raman frequencies of M1', A_{1g}'', and M3 increase under further compression, and no additional peak is observed, suggesting a stable new high-pressure phase is formed up to 57.8 GPa. We note that the Raman peaks broaden obviously at high pressure, which is due to non-hydrostatic compression associated with the pressure-transmitting medium. With pressure released down to 0.7 GPa, the peaks in the Raman spectrum return to the initial position (denoted by d, at the top of **Figure 5A**), which means that these two structural transitions are reversible, in accordance with the results of XRD data.

The extracted Raman frequencies as a function of pressure are plotted in **Figure 5B**. With increasing pressure, Raman frequencies increase linearly in each crystal structure, while the corresponding slope is visibly different. The pressure coefficients of Raman modes are fitted by linear lines using **Eq. 1** as displayed in **Figure 5B**. The individual mode Grüneisen parameter γ_i is calculated using **Eq. 2**, in which ω_i is *i*th phonon mode frequency and B_0 is the bulk modulus at zero pressure (Sherman, 1980). The corresponding results are listed in **Table 1**.

$$\omega_p = \omega_0 + \left(\frac{d\omega}{dP}\right)P \quad (1)$$

$$\gamma_i = \frac{B_0}{\omega_i} \left(\frac{d\omega}{dP}\right) \quad (2)$$

Combining the electrical transport, synchrotron XRD and Raman measurements under pressure, we established the phase diagram which describes the structural and transport properties of 1T-VSe₂ under pressure. As outlined in **Figure 6**, two critical pressure points can be discerned. With increasing pressure, T_{CDW} increases linearly at a rate of 16.5 K/GPa, suggesting that the CDW state gets strengthened with pressure in the P-3m1 phase, which is consistent with the previous report (Friend et al., 1978; Feng et al., 2020; Sahoo et al., 2020). At the first critical pressure P_{C1} ~ 12 GPa, the hexagonal P-3m1 structure undergoes a transition into monoclinic C2/m phase. The second critical pressure P_{C2} ~ 33 GPa corresponds to another structural transition from the monoclinic C2/m to P2₁/m phase. The pressure evolution of structure can also be traced by resistance measurements. One can see that the R_{10K} initially keeps a nearly constant value at low pressures. As the pressure increases up to P_{C1}, the R_{10K} suddenly goes up, while it abruptly drops around P_{C2}.

CONCLUSION

In conclusion, pressure evolutions of structure and resistance of single-crystalline 1T-VSe₂ were studied by combined high-pressure electrical transport, synchrotron XRD and Raman experiments. We demonstrate that the CDW transition in the hexagonal P-3m1 phase is enhanced remarkably by the application of pressure. And two structural phase transformation from the 1T to C2/m and from C2/m to P2₁/m is observed at P_{C1} ~ 12 and P_{C2} ~ 33 GPa, respectively. These findings will shed light on the understanding of structural and transport properties in pressurized transition metal dichalcogenides.

DATA AVAILABILITY STATEMENT

The original contributions presented in the study are included in the article/**Supplementary Material**, further inquiries can be directed to the corresponding authors.

AUTHOR CONTRIBUTIONS

MZ and XH synthesized the sample and carried out the experiments of sample characterization. DS carried out the high-pressure electrical transport measurement and high-pressure Raman scattering. YZ carried out the high-pressure X-ray diffraction measurement. XL and YZ reviewed and edited the manuscript. All authors have read and agreed to the submitted version of the manuscript.

FUNDING

This research was funded by the National Natural Science Foundation of China (NSFC) (Grant No. 11974016), Natural Science Foundation of Anhui Province (Grant No. 2008085QA40).

ACKNOWLEDGMENTS

The X-ray diffraction experiment was performed at the beamline BL15U1, Shanghai Synchrotron Radiation Facility (SSRF).

SUPPLEMENTARY MATERIAL

The Supplementary Material for this article can be found online at: <https://www.frontiersin.org/articles/10.3389/fmats.2021.710849/full#supplementary-material>

REFERENCES

- Birch, F. (1947). Finite Elastic Strain of Cubic Crystals. *Phys. Rev.* 71, 809–824. doi:10.1103/PhysRev.71.809
- Bonilla, M., Kolekar, S., Ma, Y., Diaz, H. C., Kalappattil, V., Das, R., et al. (2018). Strong room-temperature ferromagnetism in VSe₂ monolayers on van der Waals substrates. *Nat. Nanotech.* 13, 289–293. doi:10.1038/s41565-018-0063-9
- Brauer, H. E., Starnberg, H. I., Holleboom, L. J., Strocov, V. N., and Hughes, H. P. (1998). Electronic Structure of Pure and Alkali-Metal-intercalated VSe₂. *Phys. Rev. B* 58, 10031–10045. doi:10.1103/PhysRevB.58.10031
- Choi, C. L., Feng, J., Li, Y., Wu, J., Zak, A., Tenne, R., et al. (2013). WS₂ Nanoflakes from Nanotubes for Electrocatalysis. *Nano Res.* 6, 921–928. doi:10.1007/s12274-013-0369-8
- Clemens, P., and Vitali, B. P. (2015). DIOPTAS: a Program for Reduction of Two-Dimensional X-ray Diffraction Data and Data Exploration. *High Press. Res.* 35, 223. doi:10.1080/08957959.2015.1059835
- Duvjir, G., Choi, B. K., Jang, I., Ulstrup, S., Kang, S., Thi Ly, T., et al. (2018). Emergence of a Metal-Insulator Transition and High-Temperature Charge-Density Waves in VSe₂ at the Monolayer Limit. *Nano Lett.* 18, 5432–5438. doi:10.1021/acs.nanolett.8b01764
- Eaglesham, D. J., Withers, R. L., and Bird, D. M. (1986). Charge-density-wave Transitions in 1T-VSe₂. *J. Phys. C: Solid State Phys.* 19, 359–367. doi:10.1088/0022-3719/19/3/006
- Feng, J., Biswas, D., Rajan, A., Watson, M. D., Mazzola, F., Clark, O. J., et al. (2018). Electronic Structure and Enhanced Charge-Density Wave Order of Monolayer VSe₂. *Nano Lett.* 18, 4493–4499. doi:10.1021/acs.nanolett.8b01649
- Feng, J., Susilo, R. A., Lin, B., Deng, W., Wang, Y., Li, B., et al. (2020). Achieving Room-Temperature Charge Density Wave in Transition Metal Dichalcogenide 1T-VSe₂. *Adv. Electron. Mater.* 6, 1901427. doi:10.1002/aem.201901427
- Friend, R. H., Jérôme, D., Schleich, D. M., and Molinié, P. (1978). Pressure Enhancement of Charge Density Wave Formation in VSe₂; The Role of Coulomb Correlations. *Solid State Commun.* 27, 169–173. doi:10.1016/0038-1098(78)90825-6
- Ghobadi, A., Ghobadi, T. G. U., Okyay, A. K., and Ozbay, E. (2018). Emerging Photoluminescence from Defective Vanadium Diselenide Nanosheets. *Photon. Res.* 6, 244–253. doi:10.1364/PRJ.6.000244
- Guo, J., Luo, H. X., Yang, H. X., Wei, L. L., Wang, H. H., Yi, W., et al. (2017). Separation of the Charge Density Wave and Superconducting States by an Intermediate Semimetal Phase in Pressurized TaTe₂. New York: Cornell University. arXiv:1704.08106 [cond mat.supr con].
- He, S., Lin, H., Qin, L., Mao, Z., He, H., Li, Y., et al. (2017). Synthesis, Stability, and Intrinsic Photocatalytic Properties of Vanadium Diselenide. *J. Mater. Chem. A* 5, 2163–2171. doi:10.1039/C6TA10390A
- Hunter, B. A. (1998). *Rietica—A Visual Rietveld Program*. Commission on Powder Diffraction Newsletter No. 20 (Summer), International Union of Crystallography. Vienna, Austria: IAEA. Available at: <http://www.rietica.org>.
- Jolie, W., Knispel, T., Ehlen, N., Nikonov, K., Busse, C., Grüneis, A., et al. (2019). Charge Density Wave Phase of VSe₂ revisited. *Phys. Rev. B* 99, 115417. doi:10.1103/PhysRevB.99.115417
- Ma, Y., Dai, Y., Guo, M., Niu, C., Zhu, Y., and Huang, B. (2012). Evidence of the Existence of Magnetism in Pristine VX₂ Monolayers (X = S, Se) and Their Strain-Induced Tunable Magnetic Properties. *ACS Nano* 6, 1695–1701. doi:10.1021/nn204667z
- Mao, H.-K., Chen, X.-J., Ding, Y., Li, B., and Wang, L. (2018). Solids, Liquids, and Gases under High Pressure. *Rev. Mod. Phys.* 90, 015007. doi:10.1103/RevModPhys.90.015007
- Mao, H. K., Xu, J., and Bell, P. M. (1986). Calibration of the Ruby Pressure Gauge to 800 Kbar under Quasi-Hydrostatic Conditions. *J. Geophys. Res.* 91, 4673–4676. doi:10.1029/JB091iB05p04673
- Nayak, A. P., Bhattacharyya, S., Zhu, J., Liu, J., Wu, X., Pandey, T., et al. (2014). Pressure-induced Semiconducting to Metallic Transition in Multilayered Molybdenum Disulphide. *Nat. Commun.* 5, 3731. doi:10.1038/ncomms4731
- Novoselov, K. S., Mishchenko, A., Carvalho, A., and Castro Neto, A. H. (2016). 2D materials and van der Waals heterostructures. *Science* 353, aac9439. doi:10.1126/science.aac9439
- Pandey, J., and Soni, A. (2020). Electron-phonon Interactions and Two-Phonon Modes Associated with Charge Density Wave in Single Crystalline 1T-VSe₂. *Phys. Rev. Res.* 2, 033118. doi:10.1103/PhysRevResearch.2.033118
- Pásztor, Á., Scarfato, A., Barreteau, C., Giannini, E., and Renner, C. (2017). Dimensional Crossover of the Charge Density Wave Transition in Thin Exfoliated VSe₂. *2D Mater.* 4, 041005. doi:10.1088/2053-1583/aa86de
- Sahoo, S., Dutta, U., Harnagea, L., Sood, A. K., and Karmakar, S. (2020). Pressure-induced Suppression of Charge Density Wave and Emergence of Superconductivity in 1T-VSe₂. *Phys. Rev. B* 101, 014514. doi:10.1103/PhysRevB.101.014514
- Sato, T., Terashima, K., Souma, S., Matsui, H., Takahashi, T., Yang, H., et al. (2004). Three-Dimensional Fermi-Surface Nesting in 1T-VSe₂ Studied by Angle-Resolved Photoemission Spectroscopy. *J. Phys. Soc. Jpn.* 73, 3331–3334. doi:10.1143/JPSJ.73.3331
- Sereika, R., Park, C., Kenney-Benson, C., Bandaru, S., English, N. J., Yin, Q., et al. (2020). Novel Superstructure-Phase Two-Dimensional Material 1T-VSe₂ at High Pressure. *J. Phys. Chem. Lett.* 11, 380–386. doi:10.1021/acs.jpclett.9b03247
- Sherman, W. F. (1980). Bond Anharmonicities, Grüneisen Parameters and Pressure-Induced Frequency Shifts. *J. Phys. C: Solid State Phys.* 13, 4601–4613. doi:10.1088/0022-3719/13/25/005
- Si, J. G., Lu, W. J., Wu, H. Y., Lv, H. Y., Liang, X., Li, Q. J., et al. (2020). Origin of the Multiple Charge Density Wave Order in 1T-VSe₂. *Phys. Rev. B* 101, 235405. doi:10.1103/PhysRevB.101.235405
- Sipos, B., Kusmartseva, A. F., Akrap, A., Berger, H., Forró, L., and Tutiš, E. (2008). From Mott State to Superconductivity in 1T-TaS₂. *Nat. Mater.* 7, 960–965. doi:10.1038/nmat2318
- Sofer, Z., Sedmidubský, D., Luxa, J., Bouša, D., Huber, Š., Lazar, P., et al. (2017). Universal Method for Large-Scale Synthesis of Layered Transition Metal Dichalcogenides. *Chem. Eur. J.* 23, 10177–10186. doi:10.1002/chem.201701628
- Starnberg, H. I., Brauer, H. E., Holleboom, L. J., and Hughes, H. P. (1993). 3D-to-2D Transition by Cs Intercalation of VSe₂. *Phys. Rev. Lett.* 70, 3111–3114. doi:10.1103/PhysRevLett.70.3111
- Strocov, V. N., Shi, M., Kobayashi, M., Monney, C., Wang, X., Krempasky, J., et al. (2012). Three-Dimensional Electron Realm in VSe₂ by Soft-X-Ray Photoelectron Spectroscopy: Origin of Charge-Density Waves. *Phys. Rev. Lett.* 109, 086401. doi:10.1103/PhysRevLett.109.086401
- Terashima, K., Sato, T., Komatsu, H., Takahashi, T., Maeda, N., and Hayashi, K. (2003). Charge-density Wave Transition of 1T-VSe₂ studied by Angle-Resolved Photoemission Spectroscopy. *Phys. Rev. B* 68, 155108. doi:10.1103/PhysRevB.68.155108
- Thompson, A. H., and Silbernagel, B. G. (1979). Correlated Magnetic and Transport Properties in the Charge-Density-Wave States of VSe₂. *Phys. Rev. B* 19, 3420–3426. doi:10.1103/PhysRevB.19.3420
- Tsutsumi, K. (1982). X-ray-diffraction Study of the Periodic Lattice Distortion Associated with a Charge-Density Wave in 1T-VSe₂. *Phys. Rev. B* 26, 5756–5759. doi:10.1103/PhysRevB.26.5756
- Umemoto, Y., Sugawara, K., Nakata, Y., Takahashi, T., and Sato, T. (2018). Pseudogap, Fermi Arc, and Peierls-Insulating Phase Induced by 3D-2D Crossover in Monolayer VSe₂. *Nano Res.* 12, 165–169. doi:10.1007/s12274-018-2196-4
- van Bruggen, C. F., and Haas, C. (1976). Magnetic Susceptibility and Electrical Properties of VSe₂ Single Crystals. *Solid State Commun.* 20, 251–254. doi:10.1016/0038-1098(76)90187-3
- Yang, J., Wang, W., Liu, Y., Du, H., Ning, W., Zheng, G., et al. (2014). Thickness Dependence of the Charge-Density-Wave Transition Temperature in VSe₂. *Appl. Phys. Lett.* 105, 063109. doi:10.1063/1.4893027
- Zhang, D., Ha, J., Baek, H., Chan, Y.-H., Natterer, F. D., Myers, A. F., et al. (2017). Strain Engineering a 4a × √3a Charge-Density-Wave Phase in Transition-Metal Dichalcogenide 1T-VSe₂. *Phys. Rev. Mater.* 1, 024005. doi:10.1103/PhysRevMaterials.1.024005
- Zhou, Y., Chen, X., An, C., Zhou, Y., Ling, L., Yang, J., et al. (2019). Pressure-induced Irreversible Evolution of Superconductivity in PdBi₂. *Phys. Rev. B* 99, 054501. doi:10.1103/PhysRevB.99.054501

Conflict of Interest: The authors declare that the research was conducted in the absence of any commercial or financial relationships that could be construed as a potential conflict of interest.

Copyright © 2021 Song, Zhou, Zhang, He and Li. This is an open-access article distributed under the terms of the Creative Commons Attribution License (CC BY). The use, distribution or reproduction in other forums is permitted, provided the original author(s) and the copyright owner(s) are credited and that the original publication in this journal is cited, in accordance with accepted academic practice. No use, distribution or reproduction is permitted which does not comply with these terms.